Xin Yao[a], Jianfeng Gu[a], Jingping Li[b], Mingjuan Hu[a]

[a] Key Laboratory of High Temperature Materials and Tests of Ministry of Education, Shanghai Jiao Tong University, Shanghai, P. R. China

[b] Shanghai Dragon Co., Shanghai, P. R. China

Transient temperature and internal stress analysis of quenched centric and eccentric cylindrical tubes

The aim of the study is to investigate the transient temperature, structure and internal stress evolution and distribution of oil-quenched centric and eccentric cylindrical tubes by a finite element method. Thermal analysis is first performed to obtain the cooling curves for the core and surface of the tubes, and then followed by a structural analysis. The study finds that at the initial stages of the quenching process, the residual axial stresses are tensile at the surface and compressive in the core for both geometries. However, toward the end of quenching, the interactions of thermal and transformation stresses make the surface and core axial stresses of the centric tube reverse their sign several times. Under the same quenching process, it has been found that the residual stress distribution of the eccentric tube is quite different from the centric one.

Keywords: Finite element modeling; Quenching; Residual stress; Thermal analysis

1. Introduction

Temperature, microstructure and stress/strain prediction are the three main aspects of quenching simulation [1]. Generally, quenching simulation starts from a constant temperature above austenite temperature in which the structure is uniform and the internal stresses are assumed to be zero. Depending upon the cooling rate at any particular point, the decomposed austenite may transform into ferrite, pearlite, bainite or martensite, and also giving off latent heat, which affects the temperature fields in return. The intense variation of temperature, accompanied by the non-homogenous volume change due to phase transformation, gives rise to the continuous change of internal stress field. When local yield strength is exceeded for some temperature at any point in the part, non-uniform plastic flow occurs. This causes a total residual stress state at the end of the quench process that maybe beneficial or detrimental depending on the magnitude and sign of the stresses. Extreme stresses exceeding the strength limit may even break the components.

Due to the complexity of actual quenching technique for the above-mentioned reasons, researchers have identified a method to improve the situation by integrating finite element analysis (FEA) into the prediction of the residual stress. Inoue and Arimoto [2] developed the computer-aided engineering (CAE) system 'HEARTS' to calculate the coupling fields based on a metallo-thermo-mechanics theory. Denis et al. [3] reviewed the transformation plasticity and the main effects of stress on metallurgical and mechanical interaction. The development of thermal and residual stresses in quenched steel cylinders of different dimensions were studied by Schröder [4] through a finite element program. The residual stress distribution in the convex surface of the cylinders along a generating line was shown over a quarter of the cross-section and the influence of diameter and quenching conditions was discussed. Gür et al. [5–7] investigated the evolution of internal stresses and non-homogenous plastic deformation in quenching of axisymmetric components using a thermo-elastic-plastic approach, and a number of relevant process parameters during and after quenching of the components were predicted in their study. Wang et al. [8] presented a process model, including a description of the austenite-pearlite and austenite-martensite transformations in carbon steels, temperature-dependent material properties and an elastic-plastic stress analysis to investigate the quenching of 1080 carbon steel numerically, and the results were in good agreement with the corresponding measurement results.

The main objective of the present work was to investigate the internal stress distribution and evolution that occur during oil quenching of long centric and eccentric GCr15 steel tubes. GCr15 is one of the most widely used steels in engineering components such as bearing, shaft, roller and so on. Moreover, its properties are easy to acquire in a wide temperature range. The latent heat and transformation strains associated with the martensitic transformations are included in the model, along with temperature-dependent material properties. The variations of the residual stresses and strains on different surfaces and cross-sections are examined, and the effect of workpiece geometry on both the microstructure and the residual stress state is analyzed.

2. Computational model

The model for the quenching of steels consists of two parts: (1) A temperature analysis of quenching, which includes phase transformations modeling and requires a nonlinear solution procedure. (2) A stress analysis, which incorporates the thermal loads generated during the temperature analysis, as well as the transformation strains associated

with the phase changes. Only the martensitic transformation is considered in the model because experiments have shown that martensite and a little fraction of undecomposed austensite are the only final phases of oil quenching for all of the specimens. A coupled problem is assumed for temperature and stress analysis and a plane strain problem is assumed for the stress analysis. Both the temperature field and the associated internal stress distributions were calculated using a commercial FEM software MSC-Marc [9], combined with the user-defined subroutines developed by us.

2.1. Thermal and phase transformation calculation

A transient heat conduction problem with convective boundary conditions and internal heat sources is defined to calculate the temperature field. The basic heat transfer equation can be rewritten as

$$\frac{\partial}{\partial x}\left(k\frac{\partial T}{\partial x}\right)+\frac{\partial}{\partial y}\left(k\frac{\partial T}{\partial y}\right)+\dot{q}=\rho c_p\frac{\partial T}{\partial t} \tag{1}$$

where k is the thermal conductivity, ρ is the density, c_p is the specific heat per unit volume, and $\dot{q}$ is the latent heat release rate during phase transformation. The boundary and initial conditions of the problem are

$$k\frac{\partial T}{\partial x}n_x+k\frac{\partial T}{\partial y}n_y+h(T-T_\infty)=0 \tag{2}$$

and

$$T|_{t=0}=T_0(x,y,z) \tag{3}$$

respectively, where n_x and n_y are direction cosines of the respective surface normal. h stands for the temperature-dependent convective heat transfer coefficient.

The term $\dot{q}$ is related to the rate of transformation through

$$\dot{q}=\Delta H\frac{\Delta\xi}{\Delta t} \tag{4}$$

where ΔH represents the enthalpy of martensitic transformation, taken as $6.4\times10^8\,\mathrm{J/m^3}$ [10]. ξ is the volume fraction of martensite. The thermophysical properties (λ, c, ρ) are temperature-dependent and related to the volume fraction of martensite through the linear mixture rule.

Phase changes are determined for each integration point depending upon the instantaneous temperature. Only martensitic transformation is considered, and its fraction at a given temperature is estimated according to Koistinen–Marburger law [11] as

$$\xi=1-\exp[-\beta(T_{ms}-T)] \tag{5}$$

where $\beta=1.10\times10^{-2}\,\mathrm{K^{-1}}$, T_{ms} is the martensite start temperature.

2.2. Model for calculating internal stresses

A plain strain model is assumed for calculating internal stress for both geometries. When stress analysis is performed, factors to be considered include dependences of mechanical properties on temperature and volumetric dilatation that goes with transformation (transformation dilatation). Some assumptions concerning isotropic material properties have been introduced in this model for simplification.

The procedure used in the finite element program is based on an incremental approach. The incremental law governing the thermoelasticplastic behavior of the total strain increment $\mathrm{d}\varepsilon_{ij}$ is formulated as following

$$\mathrm{d}\varepsilon_{ij}=\mathrm{d}\varepsilon^e_{ij}+\mathrm{d}\varepsilon^p_{ij}+\mathrm{d}\varepsilon^v_{ij} \tag{6}$$

where $\mathrm{d}\varepsilon^e_{ij}$ and $\mathrm{d}\varepsilon^p_{ij}$ are the elastic and plastic strain increments, respectively. $\mathrm{d}\varepsilon^v_{ij}$ is the volume strain increment including the thermal and transformation strain increments.

The standard formulation of a linearly elastic problem is

$$\varepsilon^e_{ij}=\frac{1}{E}[(1+\nu)\,\sigma_{ij}-\delta_{ij}\nu\sigma_{mm}] \tag{7}$$

where the modulus of elasticity E and Poisson's ratio ν are both temperature-dependent and phase-dependent in the quenching problem, which can be described by the linear mixture rule as exemplified below for E.

$$E[T,\xi_k]=\sum_{k=\mathrm{A,M}}\xi_k E_k(T) \tag{8}$$

where A, M represent austenite and martensite, respectively.

The plastic strain increments are obtained using the classical theory of plasticity with the von Mises yield criterion and the associated flow rule

$$\mathrm{d}\varepsilon^p_{ij}=\frac{3}{2}\frac{\mathrm{d}\varepsilon^p_e}{\sigma_e}s_{ij} \tag{9}$$

The effective stress σ_e and the effective plastic strain increment $\mathrm{d}\varepsilon^p_e$ are defined as

$$\sigma_e=\sqrt{\frac{3}{2}s_{ij}s_{ij}} \tag{10}$$

and

$$\mathrm{d}\varepsilon^p_e=\sqrt{\frac{2}{3}\,\mathrm{d}\varepsilon^p_{ij}\,\mathrm{d}\varepsilon^p_{ij}} \tag{11}$$

where s_{ij} are the components of the stress deviator tensor and $\mathrm{d}\varepsilon^p_e$ is related to σ_e through the uniaxial tensile stress–strain curve.

For isotropic hardening, the stress–strain curve for the material was assumed to follow a bilinear elastic–plastic behavior with the yield stress (σ_s) corresponding to an accumulated effective plastic strain $(\overline{\varepsilon}_p)$ given by

$$\sigma_s=\sigma_{s0}+H'\varepsilon^p_e \tag{12}$$

where σ_{s0} is the initial yield stress in the current temperature, and H' is the strain hardening constant.

The thermal expansion of austenite and martensite, and the transformation strain are obtained together as incremental volume strain $\mathrm{d}\varepsilon^v_{ij}$, formulated by

$$\mathrm{d}\varepsilon^v_{ij}=\alpha\,\mathrm{d}T+\beta\,\mathrm{d}m \tag{13}$$

where α is the average thermal expansion coefficient of austenite and martensite in the mixed rule, and β is the mar-

tensite transformation expansion coefficient. dm is the fraction of martensite formed during the decrease of temperature dT.

3. Results and discussion

3.1. Finite element models and material input

Two specimens made of GCr15 steel have been examined as centrically or eccentrically drilled cylinders. Both the cylinders had identical outer (30 mm) and inner (15 mm) diameters, and the eccentricity ratio (E_r) defined by

$$E_r = S_1/S_2 \tag{14}$$

for the eccentric cylinder was 0.25, where S_1 and S_2 stand for the largest and thinnest wall thickness of the cylinders, as illustrated in Fig. 1.

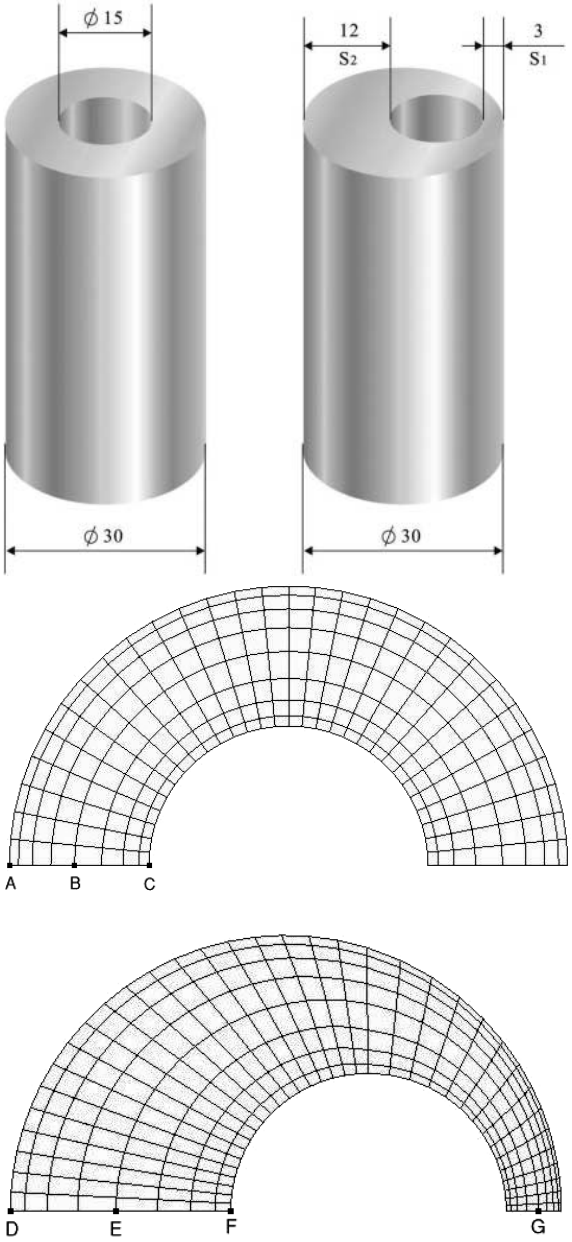

Fig. 1. (a) The geometry of the infinite long cylinders, and (b) finite element mesh of the cylinders.

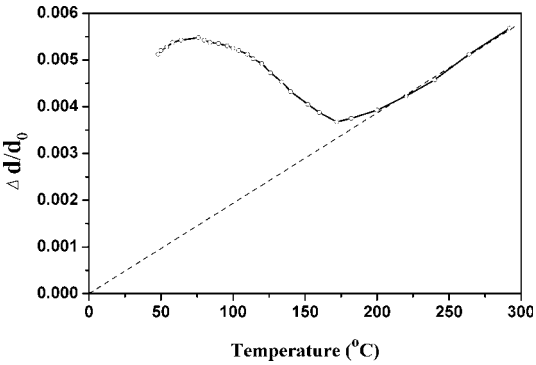

Fig. 2. Dilatation curve for GCr15 Steel.

The basic element used to produce the mesh was a plane strain arbitrary quadrilateral with four corner nodes, and with a shape function that allowed a quadratic temperature variation in any plane. Due to the symmetry of the heat flow and the geometry of the centric and eccentric tubes, it was necessary to consider only a half of an axial section, as shown in Fig. 1. The size of mesh and the bias factor required to establish instability was obtained by trial and error, and an optimized mesh size at which satisfactory results were obtained is shown in Fig. 1. The mesh near the surfaces was finer in order to improve the calculation accuracy. Owing to the symmetry, the points on the symmetry axis were restricted to displace only vertically and their displacements along the tangential direction were assumed to be zero. The thermal boundary conditions were assumed as follows: a same temperature-dependent convection heat transfer took place on the outer and inner surfaces and an adiabatic condition was set on the nodes of the symmetry axis except the surface nodes.

The expansion coefficient of austenite was obtained from the dilatometry curves shown in Fig. 2. Other mechanical and thermal properties were taken from previous publications [12] and listed in Table 1.

3.2. Temperature and martensitic transformation results

Quenching was carried out from a constant uniform temperature of 860 °C, and cooled directly to 20 °C. The quenching medium used in the experiment and simulation is the common quenching oil. Its heat transfer coefficient was determined using the inverse heat transfer coefficient methods, referring to the work of Osman and Beck [13]. The final calculated heat transfer coefficients varied with temperature are given in Fig. 3.

The cooling curves of the surface points D, F and the center points E, G for eccentric cylinder are shown in Fig. 4b. Compared to the cooling curves of corresponding points of centric cylinder in Fig. 4a, both the core and surface points D, F result in a slower cooling rate, but a larger thermal gradient during all the cooling process. Center point G of the eccentric cylinder, however, experiences a much more severe temperature change than surface points D, F, suggesting a higher thermal gradient in the eccentric cylinder. Moreover, in both cases, the outer surface point cools faster than the corresponding inner surface point though the heat transfer coefficients are the same. This is because the outer surface has a larger surface area to contact with quenching medium compared to the inner surface.

Table 1. Thermal and mechanical properties of the material used for analysis [12]; A = austenite; M = martensite.

Properties	Phases	Temperature (°C)				
		20	100	300	600	900
Specific heat capacity, C_p(W s/kgK)	A, M	553	–	787	–	729
Thermal conductivity, λ(W/mK)	A	15.0	–	18.0	21.7	25.1
	M	40.1	38.8	36.7	30.1	–
Density, ρ (kg/m^3)	A, M	7810	7810	7810	7810	7810
Thermal expansion coefficient,	A	19.5	19.5	19.5	19.5	19.5
a (10^{-6}/K)	M	10.5	10.5	10.5	10.5	–
Modulus of elasticity, E (GPa)	A	200	190	180	168	120
	M	212	206	193	165	–
Possion's ratio, v	A, M	0.3	0.3	0.3	0.3	0.3
Modulus of plasticity, H'(GPa)	A, M	3.63	3.4	3.13	2.8	2.2
Initial yield strength, σ_{s0}(MPa)	A, M	343	–	230	140	52.5

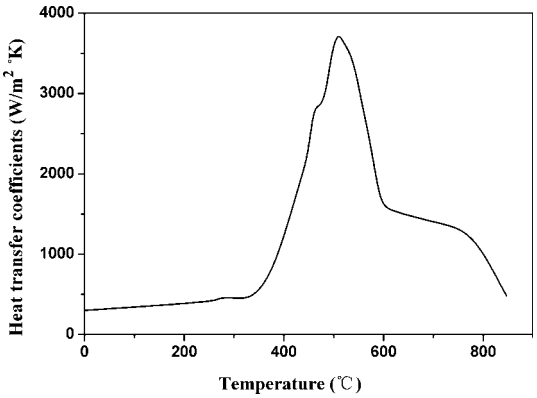

Fig. 3. Relationship between the surface temperature and the heat transfer coefficients of oil.

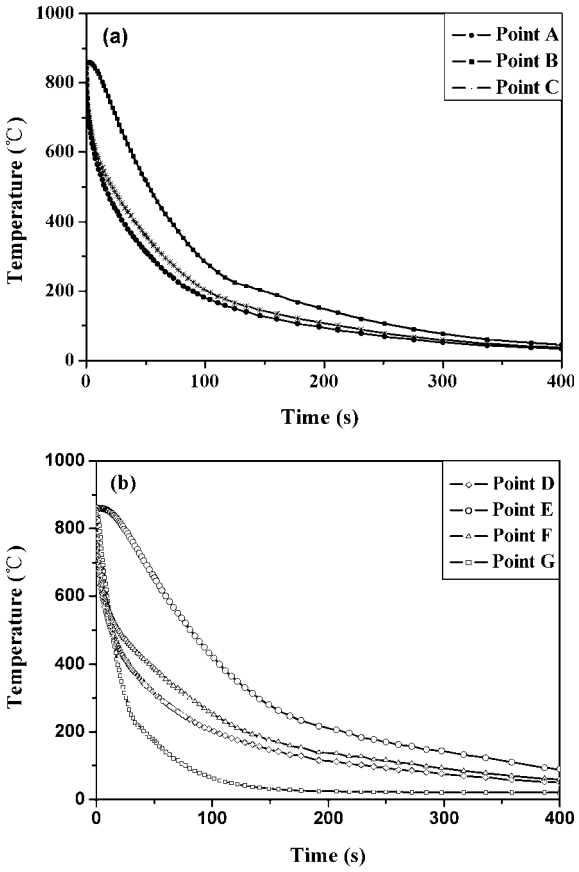

Fig. 4. Cooling curves of (a) points A, B and C of the centric cylinder, and (b) points D, E, F and G of the eccentric cylinder.

Fig. 5 shows martensitic transformation history in the centric and eccentric cylinders. Because the microstructural evolution is nonlinearly coupled to the temperature calculation via the latent heat released and the material properties of the individual phases, small changes in the temperature history can cause substantial changes in the microstructure not only at that point, but also in its vicinity within the cylinder, as is apparently shown in Fig. 4b.

It can be seen in Fig. 6a, after 400 s of oil quenching, most austenite in the centric cylinder has decomposed into martensite, though the transformation sequences are different in the surface and core points, as shown in Fig. 5a. The martensite volume fraction of the eccentric cylinder varied with time are given in Fig. 5b, and its distribution after 40 s of quenching is shown in Fig. 6b. Compared to the centric tube, the martensitic transformation sequences are more uneven, which will lead to greater residual stresses.

3.3. Stress and strain results

3.3.1. Variations of stress and strain during oil quenching of centric hollow cylinder

The intrusion of phase transformation greatly influences the stress and strain histories and distributions. To show quantitatively the dependence of stress on time during oil quenching, the same three points along the axial surface were analyzed. In the initial stage of oil quenching, the residual axial stress was tensile at the inner and outer surfaces and compressive in the core, as given in Fig. 7, but the stresses at the inner surface were slightly higher than those at the outer surface. Because of the sudden contraction of the heat transfer surface and the great temperature gradient in the vicinity of the surface, the axial stresses increase sharply to approximately 100 MPa (Fig. 8). The surface axial stress then decreases slowly with decreasing temperature gradient. The

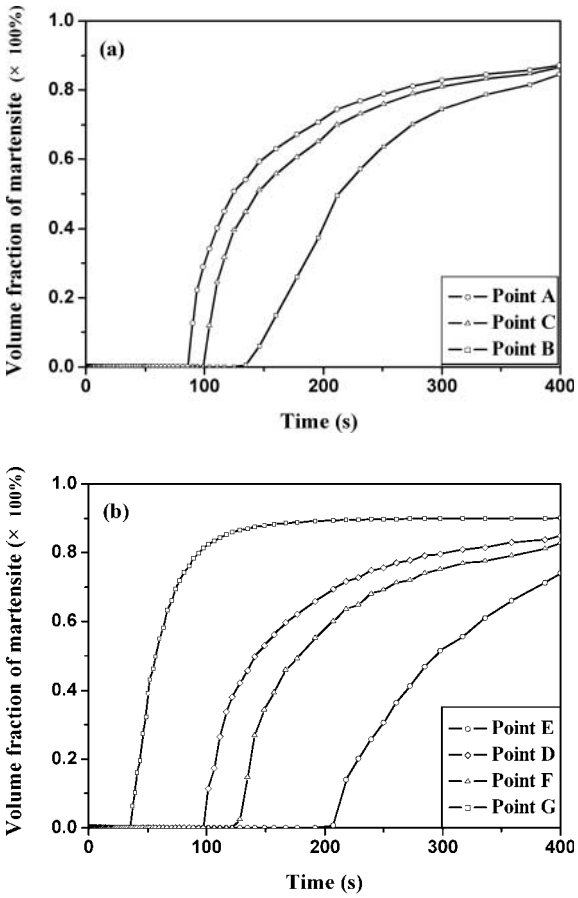

Fig. 5. Volume fraction of martensite in the (a) centric and (b) eccentric cylinders versus time.

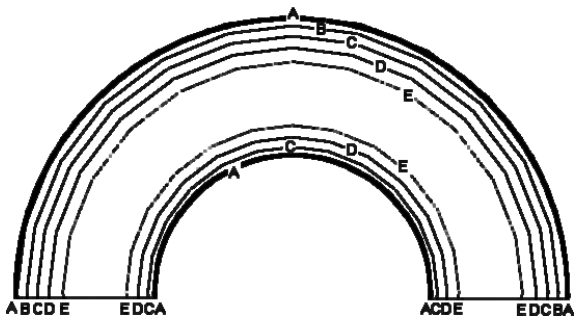

(a) A = 0.8714; B = 0.8662; C = 0.8609; D = 0.8557; E = 0.8504.

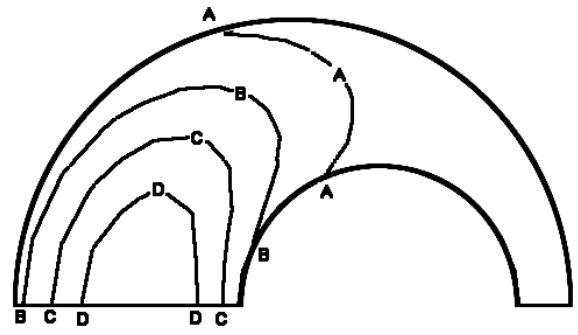

(b) A = 0.868; B = 0.837; C = 0.805; D = 0.773.

Fig. 6. Contour charts of volume fraction of martensite in the (a) centric and (b) eccentric cylinders after 400 s of oil quenching.

compressive axial stress in the core gradually increases in the initial stage, after reaching the nadir, also decreases because of the decreasing temperature gradient. If no phase transformation occurs, the surface tensile residual stress would shift to behave as compressive at a slow rate and the core compressive stress would switch into tensile stress to the end of quenching, as Sen et al. reported [14].

But actually, before the reversal of the sign of stress, martensitic transformation took place first at about 80 s at the outer surface after its temperature reached martensite start point (see Fig. 5a). Because the martensitic transformation expansion coefficient (0.9849 %) is much higher than the thermal expansion coefficient (1.9093×10^{-5}/K for austenite and 1.0564×10^{-5}/K for martensite), the martensite transformation expansion switched the surface tensile stress into compressive stress at a high rate. At the same time, the martensitic transformation in the core has not taken place and the surface expansion introduced a great tensile stress that may exceed the yield limit. With the temperature decreased, the transformed zone extended inwards, and the martensite formation near the surface reversed the surface stress to positive at about 120 s. The core tensile stress was greatly relaxed after the martensitic transformation begins, then at about 280 s, the axial stress reversed the sign to negative. The final axial stress, as given in Fig. 7, is tensile at outer and inner surfaces and compressive in the core.

Fig. 9 shows the variation of total axial strain at surface point A, including elastic strain ε^e, plastic strain ε^p, thermal

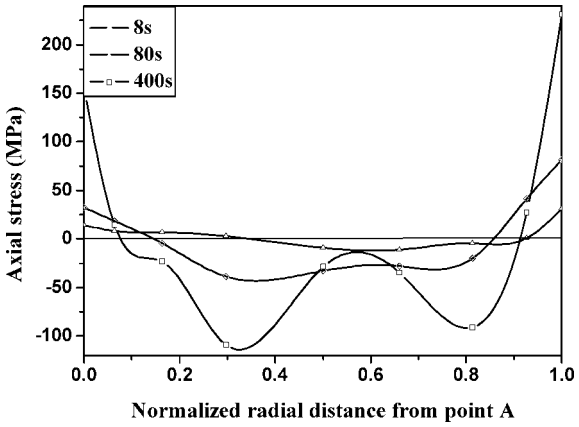

Fig. 7. Distribution of the axial stress in the centric cylinder.

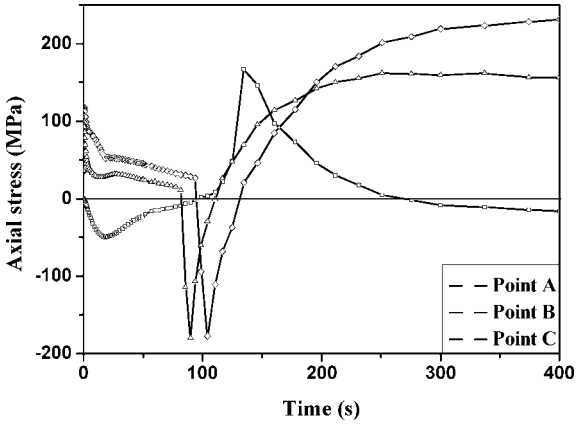

Fig. 8. Evolution of the axial stress during oil quenching.

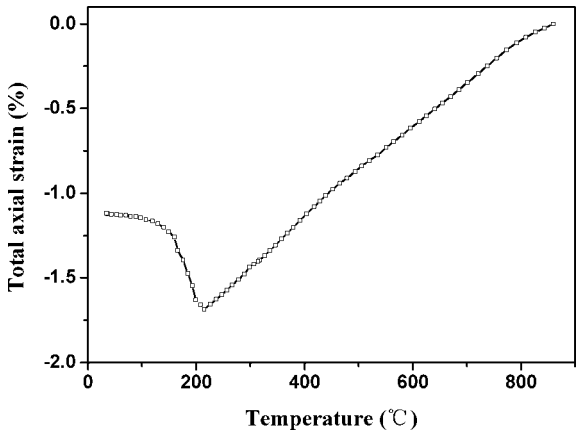

Fig. 9. Variation of the total axial strain at surface point A versus temperature.

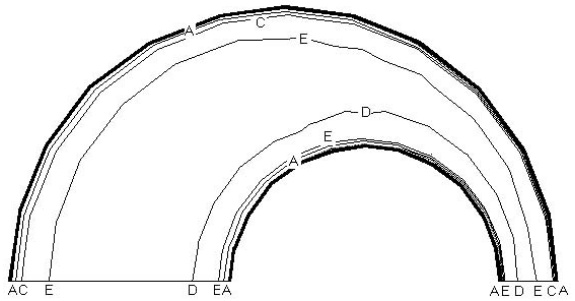

(a) A = 260 MPa; B = 170 MPa; C = 78 MPa; D = −12 MPa; E = −103 MPa.

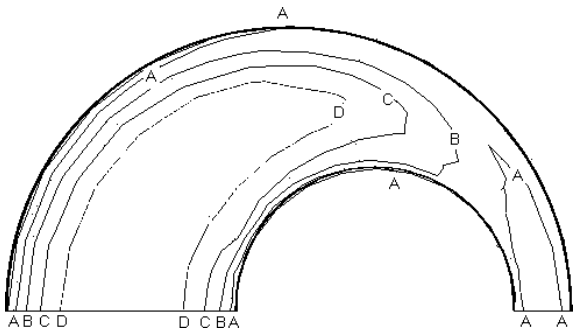

(b) A = 257 MPa; B = 190 MPa; C = −75 MPa; D = −134 MPa.

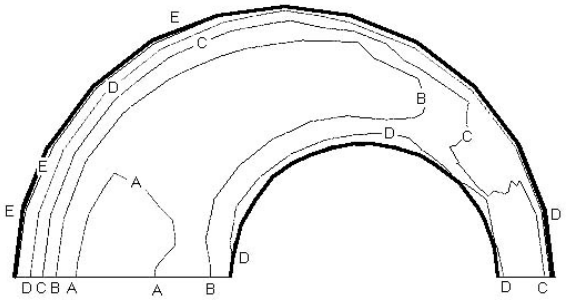

(c) A = 120 MPa; B = 40 MPa; C = −40 MPa; D = −120 MPa; E = −200 MPa.

Fig. 10. Contour charts of the axial stress in the eccentric cylinder after (a) 0.8 s, (b) 15 s, and (c) 400 s of oil quenching.

and transformation strain ε^{v}, with time during oil quenching. As can be seen from the figure, in the initial stage of quenching, the thermal strain dominate the total strain, but after martensitic transformation occurs in 230 °C, the curve goes up sharply revealing a prominent expansion of surface point A.

3.3.2. Variation of stress and strain during quenching of eccentric cylinders

The stress and strain variation during quenching of the eccentric hollow cylinder is more complicated than the centric one because of the asymmetric geometry and the interaction of the thermal and transformation stresses.

A brief process of the axial stress evolution of quenching the eccentric cylinder is depicted in Fig. 10. In the first stage of oil quenching, as depicted in Fig. 10a, only thermal stress is presented, and the surface is in tension while the core is in compression. In the second stage (Fig. 10b), because the temperature of the thinner section of the cylinder drops much faster than that of the thicker section, a complete tensile stress is presented from the surface to the core of the thinner section. Then, the thinner part of the section, also because of the faster temperature decrease, transforms into martensite almost completely in a short time. The transformation expansion put the thinner section in compression and the core of the thicker section in tension, though later transformation in the core greatly reduced the magnitude of the tensile stress. The stress state after 400 s of oil quenching is given in Fig. 10c.

Oil quenching is less intense than water quenching, and the residual stress is comparatively small. In the initial stage of quenching, because the entire piece is composed of austenite that has high ductility, the possibility of cracking is small even undergoing great plastic deformation. But in the later stage, the sudden expansion due to martensite formation reverse the stress sign and induce great internal stress to the border of the transformed and untransformed region. The surface, being martensite and having reached room temperature much earlier, will prevent the core from expanding or contracting as much as it should. This will greatly increase the possibility of large deformation or even cracking.

4. Conclusions

The transient temperature, structure and residual stress distribution and evolution of both centric and eccentric cylindrical tubes during oil quenching have been investigated using the finite element method. The results show that the temperature gradient in the eccentric tube is higher than that in the centric one during the whole oil quenching process, though the heat transfer convective boundary conditions are the same. Accordingly, the martensitic transformation sequences are much more uneven in the eccentric tube. The interaction between thermal and transformation stress makes the axial residual stress both at the surfaces and in the core reverse the sign several times during quenching the centric tube. Axial stress in the thinner section of the eccentric tube is tensile from the surface to the core at the initial stage of quenching, but after martensitic transformation begins, it reverses the sign to compressive because of the transformation expansion.

References

1. J. Pan, Y. Li, D. Li: J. Mater. Proc. Technol. 122 (2002) 241.
2. T. Inoue, K. Arimoto: J. Mater. Eng. Perf. 6 (1997) 51.
3. S. Denis, E. Gautier, A. Simon, G. Beck: Mater. Sci. Technol. 1 (1985) 805.
4. R. Schröder: J. Mater. Sci. Technol. 1 (1985) 754.
5. C.H. Gür, A.E. Tekkaya: Steel Research 67 (1996) 298.
6. C.H. Gür, A.E. Tekkaya, W. Schuler: Steel Research 67 (1996) 501.
7. C.H. Gür, A.E.Tekkaya: Mater. Sci. Eng. A 319–312 (2001) 164.
8. K.F. Wang, S. Chandrasekar, H.T. Yang: J. Manufact. Sci. Eng. 119 (1997) 257–265.
9. Marc user's manuals. Marc Analysis Research Corporation, Palo Alto, USA, Chapters A 5-8-A 5-91.
10. H. Cheng, X. Huang, H. Wang: J. Mater. Proc. Technol. 89–90 (1999) 339.
11. D.P. Koistinen, R.E. Marburger: Acta Metall. 7 (1959) 59.
12. S. Zhong, C. Wang: Bearing Steel, Metallurgical Industry Press, Beijing (2000), 119 [in Chinese].
13. A.M. Osman, J.V. Beck: J. Heat Transfer 112 (1990) 843.
14. S. Sen, B. Aksakal, A. Ozel: Int. J. Mechanical Sci. 42 (2000) 2013.

(Received July 8, 2002)

Correspondence address

Xin Yao
560#, Dept. of Mater. Sci. & Eng., Shanghai Jiao Tong University
1954 Huashan Rd., Shanghai, P. R. China
Tel.: +86 21 6293 2563
Fax: +86 21 6293 2563-8015
E-mail: xin_yao@yahoo.com